DTU Library

Active Fault Current Limitation for Low-Voltage Ride-Through of Networked Microgrids

Liu, Xubin; Chen, Xinyu; Shahidehpour, Mohammad; Li, Canbing; Wu, Qiuwei; Wu, Yuhang; Wen, Jinyu

Link back to DTU Orbit

Active Fault Current Limitation for Low-Voltage Ride-Through of Networked Microgrids

Xubin Liu, *Member*, *IEEE*, Xinyu Chen, *Member*, *IEEE*, Mohammad Shahidehpour, *Fellow*, *IEEE*, Canbing Li, *Senior Member*, *IEEE*, Xia Chen, *Senior Member*, *IEEE*, Jinyu Wen, *Member*, *IEEE*, Yuhang Wu, Qiuwei Wu, *Senior Member*, *IEEE*

Abstract—With the continuously increasing penetration of networked microgrids (MGs) on the local utility grid (UG), MGs face the challenge to avoid increasing system fault currents during low-voltage ride-through (LVRT). To solve this challenge, an active fault current limitation (AFCL) method is proposed with three parts: 1) a novel phase angle adjustment (PAA) strategy is conducted to relieve the impact of MGs output fault current on system fault current; 2) the current injection (CI) strategy for LVRT is formulated to fit the function of PAA; 3) a novel converter current generation (CCG) strategy is developed to achieve a better voltage support ability by considering network impedance characteristics. The proposed AFCL method is applied to the back-to-back converter, as a connection interface between MGs and UG. Extensive tests and pertinent results have verified the improvements of proposed AFCL method with better LVRT performance, while the networked MGs output fault current does not increase the amplitude of system fault current.

Index Terms—Networked microgrids, back-to-back converter, low-voltage ride-through, fault current limitation.

NOMENCLATURE

Abbreviations

LVRT	Low-voltage ride-through
AFCL	Active fault current limitation
PAA	Phase angle adjustment
CI	Current injection
CCG	Converter current generation
BTB	Back-to-back
PCC	Point of common coupling
GSC	Grid side converter in BTB
MSC	Microgrid side converter in BTB

Indices and superscripts

$*$	Reference value
$\wedge$	Amplitude value
N	Rated value
$+, -$	Positive/negative sequence
α, β	Variables in stationary reference frame
q, p	Reactive/active current/power
l, m, M	l^{th}, m^{th}, M^{th} MGs

Parameters and variables

I_{mq}, I_{mp}	Injected reactive/active current for LVRT
U_0, U_F, U_N	Pre-fault voltage, post-fault voltage, rated voltage
I_{max}, I_N	Converter's maximum/rated current
k^+_{LVRT} / k^-_{LVRT}	Adjustable coefficients for grid code of LVRT
$\theta^{+/-}_m$	PAA for m^{th} MG fault current
$\delta_{UG}, \delta_{PCC}$	Voltage phase angle difference from UG and MGs to fault branch
R_m, X_m	Network impedance from m^{th} MG to fault bus
R_{UG}, X_{UG}	Network impedance from UG to fault bus
U^+, U^-	Positive/negative sequence voltage amplitude
u^+, u^-	Positive/negative sequence voltage vector
ω	UG angular frequency
$i_{m\alpha(p)}, i_{m\beta(p)},$ $i_{m\alpha(q)}, i_{m\beta(q)}$	Reactive/active current in stationary reference frame
k^+_p, k^-_p k^+_q, k^-_q	Positive and negative sequence adjustable coefficients for CCG strategy
u_{dc}	DC voltage in BTB converter

X. Liu, X. Chen, X. Chen, and J. Wen are with the School of Electrical and Electronic Engineering, Huazhong University of Science and Technology, Wuhan 430074, China (e-mail: liuxubin@hust.edu.cn, xchen2019@hust.edu.cn). Mohammad Shahidehpour is with the Electrical and Computer Engineering Department, Illinois Institute of Technology, Chicago, IL 60616 USA, and also with the Center of Research Excellence in Renewable Energy and Power Systems, King Abdulaziz University, Jeddah 21589, Saudi Arabia (e-mail: ms@iit.edu). C. Li and Y. Wu are with the School of Electronic Information and Electrical Engineering, Shanghai Jiao Tong University, Shanghai 200240, China (e-mail: licanbing@sjtu.edu.cn). Q. Wu is with the Center for Electric Power and Energy (CEE), Department of Electrical Engineering, Technical University of Denmark (DTU), 2800 Kgs. Lyngby, Denmark (e-mail: qw@elektro.dtu.dk).

I. INTRODUCTION

MICROGRIDS (MGs) are commonly regarded as an efficient platform to aggregate a cluster of geographically close distributed generators (DGs) and loads [1]. With increasing integration level of distributed energy resources, MGs are interconnected as a networked MGs system, forming a promising solution for refining energy and providing ancillary services in the local distribution networks [1]. Among these services, the LVRT of networked MGs, which requires MGs to maintain connected with UG during voltage sags, plays a more crucial role than ever before, since the numbers and capacity of MGs have been continuously increasing [2]-[3].

Most of the existing LVRT practices are applied for DGs (e.g., wind farms and photovoltaic arrays) [4]-[6]. It is meaningful to study the LVRT of networked MGs since its unplanned islanding mode will cause some serious problem: 1) There will be an un-ignored capacity reduction of UG, which

may lead to the invalidity of the original dispatch plan [7]; 2) There will be a further deterioration of UG voltage amplitude and frequency fluctuations if networked MGs are disconnected suddenly [8]; 3) The power supply of critical load in MGs will not be guaranteed if the power generation in MGs is insufficient [9]; 4) The excessive power generation in MGs will be wasted when the power cannot be delivered to UG; besides, the energy storage system might be fully charged [10]; 5) After fault is cleared, the reconnection of MGs would cause large inrush current and synchronization problems [11].

The LVRT of MGs is essentially necessary. However, this LVRT ancillary service will bring a serious challenge of monotonically increasing system fault current because MGs will contribute fault current to fault branch along with the UG [12]. Considering that MGs fault current is an additional and adverse current, it is imperative to reduce the impact of MGs fault current, in order to keep the system fault current level unchanged [12]. Otherwise, the increased part of fault current will cause serious consequences when system fault current exceeds the maximum endurance of electric equipment [12]-[13]. First, the injection of MGs fault current will lead to the costly upgrades of grid components, such as transmission lines, transformers, circuit breakers, and fuses [14]. Second, the additional MGs fault current will increase the difficulty of relay protection, even causing protection failure and catastrophic damage, which would threaten grid security and stability [15]. Third, the high-level fault current will increase the electromagnetic interference to fault surrounding area, and severely affect personal and equipment safety [16].

Numerous studies have been developed to conquer DGs' and MGs' impact on system fault current during its LVRT. One is passive methods. The advanced protection equipment, such as inverse time admittance relay, are equipped and upgraded to accommodate the increase of fault current [17]. Considering protection communications problem, the phasor measurement unit (PMU) strategy and agent-based protection strategy are also proposed in [18]. To avoid large-scale updates of protection devices and communication equipment, fault current limiters are adopted to attenuate the impact of DGs fault currents [13], [19]. The others represent active methods. Initially, based on IEEE Std 1547−2003 and IEEE Std 929−2000, the DGs and MGs are disconnected once UG faults occur [20]. Then, the capacity threshold strategy with considering the size and location of DGs is studied to limit the DGs output fault current [21]. After that, since the voltage sags will increase the peak value of inverter output current under the same power injection, the peak current limitation strategy is proposed for DGs to avoid sudden tripping of grid-tied inverter [22]. However, the core essence of above active methods is to protect the grid-tied inverter itself, since inverter can only withstand 2~3 times rated current [23]-[24]. Based on superposition theorem of sinusoidal current, the DGs will inevitably increase system fault current, when phase angles of different injected fault current are basically the same or with small difference.

More than focusing on inverter protection, the increasing fault current in system level becomes a challenge. Recently, in order to weaken the influence of DGs on system fault current during its LVRT, the phase angle adjustment of DGs fault current is proposed to make DGs and UG fault currents have a certain phase angle difference [23]-[25]. However, although the system fault current amplitude will be lower than the sum of DGs and UG fault current amplitude, it is still significantly larger than UG fault current amplitude [23]-[25]. Why system fault current cannot be equal to UG fault current is the inaccurate phase angle adjustment. In practical systems, the fault occurs arbitrarily, while the voltage/current sampling points of PCC and UG are generally fixed based on PMU or the other sensor detection devices. Considering the long line distances from MGs and UG to fault branch, one of the most critical factors for phase angle adjustment is to comprehensively consider the phase angle differences on the realistic line impedance. Therefore, a novel PAA strategy is conducted to completely eliminate the impact of MGs fault current by considering voltage's phase angle differences from UG to fault branch and from MGs to fault branch.

In practice, most of the existing MGs/DGs interact flexibly to UG via the simple PCC connection interface, such as electro-mechanical circuit breakers and solid-state switches [26]. Although these interfaces require a simple structure and less investment, the BTB converter becomes more attractive, since it can not only achieve a flexible and reliable bidirectional power flow, but also isolate the frequency and voltage fluctuation between UG and MGs [27]. In industrial distribution networks, with the high demand for power quality of both UG and MGs, the BTB converter is widely used to meet customers' requirements that have a large proportion of sensitive loads, such as chemical plants and semiconductor devices [9]. Therefore, the reason why we apply BTB converters to connect MGs and UG is to deal with these special scenarios with high demand power quality. The inverter dominated MGs that are equipped by BTB converter can be considered as a centralized power source. In order to achieve the trade-off between LVRT and the active fault current limitation, the CI strategy for the grid code requirement of LVRT is conducted to fit the function of the PAA strategy.

The key of LVRT is to control PCC voltage, which relates to the output current of the BTB converter and the network impedance. This impedance is respectively assumed as pure inductive, pure resistive, and resistive-inductive in medium/high voltage network, low voltage network, and the complex network [2]-[3], [13]. The network impedance can greatly affect the amplitude/phase angle of PCC voltage [2]-[3], [19]-[20], [23]-[25]. Numerous studies have been developed to improve CCG by considering network impedance [28]-[30]. What they have in common is to consider impedance as feedforward/feedback control loops in CCG, such as (virtual) impedance control, and harmonic resonant regulator [28]-[30]. Different from feedforward/feedback loops [28]-[30], directly embedding impedance to CCG controller will be interesting. For the purpose of achieving a better PCC voltage support ability during the LVRT of networked MGs, a novel CCG strategy is developed by embedding the network impedance characteristics.

The motivation of this paper is to avoid monotonically increasing system fault currents during the LVRT of networked MGs. To solve this challenge, an AFCL method is proposed to relieve the impact of MGs fault current. The major contributions are outlined as: 1) a novel PAA strategy is conducted for MGs output fault current with considering voltage's phase angle differences from UG to fault branch and from MGs to fault branch, in order to keep the amplitude of system fault current unchanged; 2) the CI strategy is conducted to fit the function of PAA under the requirement of LVRT grid code; 3) a novel CCG strategy is developed to improve the LVRT performance by embedding network impedance characteristics.

The remainder of this paper is organized logically. The fault current requirements during LVRT is formulated in Section II. An AFCL method consists of PAA, CI, and CCG strategies are conducted in Section III. Comparative tests with AFCL during LVRT of networked MGs are developed in Section IV. The conclusion is provided in Section V.

II. FAULT CURRENT REQUIREMENTS DURING LVRT OF NETWORKED MGs

Before fault current limitation, it is necessary to analyze the fault current requirements during LVRT of networked MGs.

A. System Fault Current Flow

The PCC connection interface of networked MGs is designed as a BTB converter, which consists of grid side converter (GSC) and MG side converter (MSC). The UG and MGs are considered as uniform power sources. During LVRT of networked MGs, all MGs inject fault current into fault branch along with UG [23]-[25]. The structure of networked MGs and the flow path of fault currents are shown in Fig. 1.
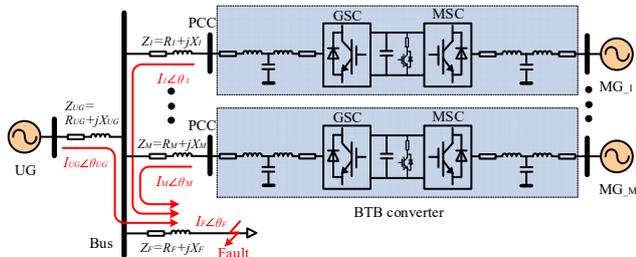

Fig. 1. Structure of networked MGs and the corresponding fault current flow.

Based on Fig. 1, Z_{UG} is the network impedance from UG to fault bus, Z_1 and Z_M are the impedance from I^{th} and M^{th} MG to fault bus. Z_F is the impedance in fault branch. The I_{UG}, I_1, I_M and θ_{UG}, θ_1, θ_M are the amplitude and phase angle of UG fault current, I^{th} and M^{th} MG fault current. The I_F and θ_F are the amplitude and phase angle of system fault current.

During LVRT of networked MGs, the system fault current is described as

$$I_F = \frac{Z_1 // ... // Z_M}{Z_1 // ... // Z_M + Z_F} I_{UG} + \frac{Z_{UG}}{Z_{UG} + Z_F}(I_1 + ... + I_m + ... + I_M). \quad (1)$$

For the low-impedance fault ($Z_F << Z_1 // ... // Z_M$, $Z_F << Z_{UG}$) [25], then, the I_F is further approximated as

$$I_F = I_{UG} + (I_1 + ... + I_m + ... + I_M). \quad (2)$$

According to (2), the system fault current amplitude is much greater than that in case without MGs ($I_F = I_{UG}$).

B. Fault Current Injection by Grid Code Requirement

The grid code requirement for the LVRT operation is shown in Fig. 2. In Fig. 2(a), different countries have different grid code requirements to withstand voltage sags during LVRT. After comparison, the German's E.ON NetZ code is adopted, due to its strict requirements [2]-[3]. Once PCC voltage sags below the red curve, MGs are allowed to disconnect from UG [2]-[3]. Otherwise, MGs should remain connected by injecting a certain reactive current. In Fig. 2(b), when the PCC voltage falls below 90% of rated voltage, each 1% positive sequence voltage sag requires to inject at least k_{LVRT}% increment of positive sequence reactive current. If needed, it is required to inject 1 p.u. of reactive current. Thus, the requirement of positive sequence reactive current for the mth MG is estimated as

$$I_{mq}^+ = \begin{cases} 0, & U_F^+ \in (0.9U_N, 1.2U_N] \\ k_{LVRT}^+ \times \left(\dfrac{U_N - U_F^+}{U_N} \right) \times I_N, & U_F^+ \in (0.5U_N, 0.9U_N] \\ I_N, & U_F^+ \in (0, 0.5U_N] \end{cases} \quad (3)$$

However, there is still no unified mechanism about negative sequence reactive current requirement. In unbalanced fault voltage sag, in order to provide a satisfactory LVRT and system protection, the negative sequence reactive current can be consistent with the positive sequence. When the voltage drops low (e.g., lower than 0.5 p.u.), the requirements of positive sequence reactive current should be satisfied first based on grid code, while negative reactive current is set to be zero. That is, the LVRT should give priority to PCC voltage support, rather than voltage balance. When the fault voltage ranges from 0.5~0.9 p.u., similar to (3) and based on the analysis in [31], the negative sequence current is injected in proportion to negative sequence voltage. Thus, the negative sequence reactive current can be estimated as

$$I_{mq}^- = \begin{cases} 0, & U_F^+ \in (0.9U_N, 1.2U_N] \\ k_{LVRT}^- \times \left(\dfrac{-U_F^-}{U_N} \right) \times I_N, & U_F^+ \in (0.5U_N, 0.9U_N] \\ 0, & U_F^+ \in (0, 0.5U_N] \end{cases} \quad (4)$$

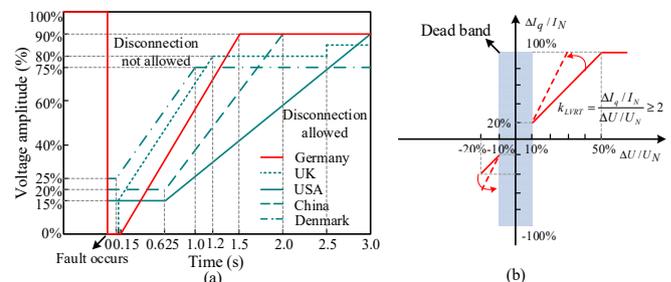where $k_{LVRT}^{+/-} \geq 2$, according to German grid code [2]-[3], [32].

Fig. 2. Grid code requirements. (a) LVRT protocols of different countries for the tolerance of voltage sags, (b) Positive sequence reactive current requirement by Germany.

III. ACTIVE FAULT CURRENT LIMITATION METHOD FOR LVRT OF NETWORKED MGS

The behavior of LVRT of networked MGs is determined by the performance of the BTB converter. To relieve the contribution of MGs fault current on system fault current, an AFCL method is proposed with PAA, CI, and CCG strategies.

A. PAA Strategy

Based on Fig. 1, system fault current is formed by adding UG fault current and MGs fault current. The UG fault current is synchronous and non-adjustable, while the MGs fault current can be controlled through the BTB converter. Based on the GSC, the MGs fault current has the controllable variables, including amplitude and angle. Based on the same amplitude, the contribution of MGs fault current on system fault current depends on its phase angle [23]-[25]. Taking one of MG as an example, the vector analysis of fault voltage/current without/with PAA strategy is displayed in Fig. 3.
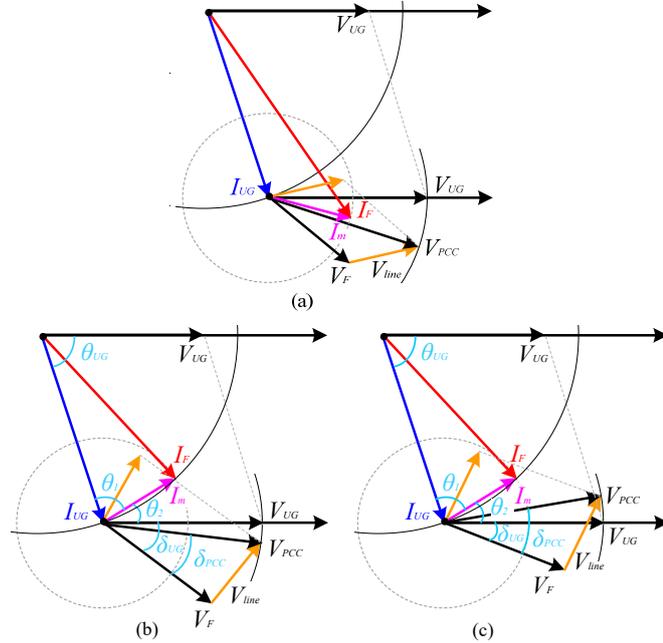

Fig. 3. Fault voltage and current vector analysis: (a) without PAA strategy, (b) with PAA strategy under *scenario 1*, (c) with PAA strategy under *scenario 2*.

There are two scenarios in the case of PAA. The Fig. 3(b) represents *scenario 1*: the voltage's phase angle difference from UG to fault branch (δ_{UG}) is larger than that from MG to fault branch (δ_{PCC}). The Fig. 3(c) represents *scenario 2*: the δ_{UG} is smaller than δ_{PCC}. Since the principle of PAA in positive/ negative sequence is the same, the vectors and variables are not distinguished in sequences in Fig. 3. The V_{UG}, V_F, and V_{PCC} are the normal voltage, fault voltage at fault branch, PCC voltage during LVRT of mth MG. The phase angle of MG fault current (I_m) lags the phase angle of voltage formed on network impedance (V_{line}) due to its inductance features. However, similar characteristics exist in both scenarios. In the case without or with PAA, the phase angle of I_m is different, thus the phase angle of V_{PCC} is different. In the case without or with PAA, the amplitude of V_{PCC} should be equal to V_{UG}, and the system fault current (I_F) is to the same as vector summation of UG fault current (I_{UG}) and m^{th} MG fault current (I_m). However,

in case without PAA, the I_F is much larger than I_{UG}; while, in the case with PAA, the I_F is equal to I_{UG}. Thus, the contribution of MG's fault current on system fault current is relieved by the PAA strategy no matter what kind of scenarios.

Based on the analyses of Fig. 3, the key of PAA is to calculate and determine the feasible phase angle of mth MG fault current (I_m). During voltage and current sampling, the phase angle of I_m and I_{UG} is referenced to the phase angle of V_{PCC} and V_{UG}. Considering the long line distances from MGs to UG, there is a non-negligible angle between V_{PCC} and V_{UG}. However, the phase angles of V_{PCC} and V_{UG} are simply assumed to be the same in the existing method [23]-[25]. To improve the mitigation ability of MG fault current, we propose a novel PAA strategy by considering voltage's phase angle differences from UG to fault branch (δ_{UG}) and from MGs to fault branch (δ_{PCC}).

As shown in Fig. 3, the system fault current with PAA strategy is expressed as

$$\vec{I}_{UG}^{+/-} + \vec{I}_{m}^{+/-} = \vec{I}_{F}^{+/-} \quad . \tag{5}$$

The amplitude relationship is described as

$$\hat{I}_{F}^{+/-} = \hat{I}_{UG}^{+/-} \quad . \tag{6}$$

According to (6), the (5) can be rewritten as

$$\begin{cases} \hat{I}_{UG}^{+/-}\cos(\theta_{UG}^{+/-}) + \hat{I}_{m}^{+/-}\cos(\theta_{2}^{+/-}) = \hat{I}_{UG}^{+/-}\cos(\theta_{F}^{+/-}) \\ \hat{I}_{UG}^{+/-}\sin(\theta_{UG}^{+/-}) + \hat{I}_{m}^{+/-}\sin(\theta_{2}^{+/-}) = \hat{I}_{UG}\sin(\theta_{F}^{+/-}) \end{cases} . \tag{7}$$

According to geometric relationship in Fig. 3, there is

$$\theta_{1}^{+/-} + \theta_{2}^{+/-} + \theta_{UG}^{+/-} = 180^{\circ} . \tag{8}$$

Then

$$\theta_{2}^{+/-} = 180^{\circ} - \theta_{UG}^{+/-} - \cos^{-1}(\frac{\hat{I}_{m}^{+/-}}{2\hat{I}_{UG}^{+/-}}) . \tag{9}$$

Based on Fig. 3(b)-(c), considering the voltage's phase angle difference of δ_{UG} and δ_{PCC} under *scenario 1* and *scenario 2*, the feasible phase angle of I_m is expressed as

$$\theta_{m}^{+/-} = \begin{cases} \theta_{2}^{+/-} + (\delta_{UG}^{+/-} - \delta_{PCC}^{+/-}), & \delta_{UG}^{+/-} > \delta_{PCC}^{+/-} \\ \theta_{2}^{+/-} - (\delta_{UG}^{+/-} - \delta_{PCC}^{+/-}), & \delta_{UG}^{+/-} < \delta_{PCC}^{+/-} \end{cases} . \tag{10}$$

Considering the nature of $\theta_{m}^{+/-}$, there exists

$$\hat{I}_{m}^{+/-} = \frac{\hat{I}_{mq}^{+/-}}{\sin(\theta_{m}^{+/-})} . \tag{11}$$

Based on (10)-(11), the (9) is rewritten as

$$\theta_{m}^{+/-} = 180^{\circ} - \theta_{UG}^{+/-} - \cos^{-1}(\frac{\hat{I}_{mq}^{+/-}}{2\hat{I}_{UG}^{+/-}\sin(\theta_{m}^{+/-})}) \pm (\delta_{UG}^{+/-} - \delta_{PCC}^{+/-}) . \tag{12}$$

Then, the (12) is rewritten as

$$\sin(\theta_{m}^{+/-})\cos[180^{\circ} - \theta_{UG}^{+/-} \pm (\delta_{UG}^{+/-} - \delta_{PCC}^{+/-}) - \theta_{m}^{+/-}] = \frac{\hat{I}_{mq}^{+/-}}{2\hat{I}_{UG}^{+/-}} . \tag{13}$$

Based on the mathematical transformation of (12), under *scenario 1* and *scenario 2*, the novel PAA strategy with considering voltage's phase angle differences from UG to fault branch and from MGs to fault branch is proposed as

$$\theta_{m}^{+/-} = \frac{1}{2}\{[180^{\circ} - \theta_{UG}^{+/-} \pm (\delta_{UG}^{+/-} - \delta_{PCC}^{+/-})] + \\ \sin^{-1}[\frac{\hat{I}_{mq}^{+/-}}{\hat{I}_{UG}^{+/-}} - \sin(180^{\circ} - \theta_{UG}^{+/-} \pm (\delta_{UG}^{+/-} - \delta_{PCC}^{+/-}))]\} . \tag{14}$$

This article has been accepted for publication in a future issue of this journal, but has not been fully edited. Content may change prior to final publication. Citation information: DOI 10.1109/TPWRD.2021.3074992, IEEE Transactions on Power Delivery

5

B. CI Strategy

In order to adjust the phase angle of BTB converter output current to fit the PAA strategy, the active current should be injected with a certain angle ($\theta_m^{+/-}$). Based on (3) and (11), the requirement of active current for the mth MG are proposed as

$$I_{mp}^{+/-} = \begin{cases} 0, & U_F^+ \in (0.9U_N, 1.2U_N] \\ \dfrac{I_{mq}^{+/-}}{\tan(\theta_m^{+/-})}, & U_F^+ \in (0, 0.9U_N] \end{cases} \quad (15)$$

Based on (3) and (15), to avoid tripping of BTB converter during LVRT. The BTB converter output current is limited as

$$I_{peak} = \frac{2}{3}\sqrt{(I^+)^2 + (I^-)^2 + 2I^+I^-} = \frac{2}{3}(I_m^+ + I_m^-)$$
$$= \frac{2}{3}\left(\sqrt{(I_{mq}^+)^2 + (I_{mp}^+)^2} + \sqrt{(I_{mq}^-)^2 + (I_{mp}^-)^2}\right) \le I_{\max} \quad (16)$$

where I_{max} is the maximum current, which is limited to 2~3 times I_N in silicon devices [23]-[24].

According to [13], and based on (3)-(4) and (15), ignoring oscillatory terms of instantaneous active/reactive power, the reference injected active/reactive power is obtained as

$$P_m^* = \frac{3}{2}(U^+ I_{mp}^+ + U^- I_{mp}^-)$$
$$Q_m^* = \frac{3}{2}(U^+ I_{mq}^+ + U^- I_{mq}^-) \quad (17)$$

C. CCG Strategy

The active/reactive powers of mth MG is injected as

$$\begin{bmatrix} P_m \\ Q_m \end{bmatrix} = \frac{3}{2}\begin{bmatrix} u_\alpha & u_\beta \\ u_\beta & -u_\alpha \end{bmatrix}\begin{bmatrix} i_{m\alpha} \\ i_{m\beta} \end{bmatrix}. \quad (18)$$

Based on (18), and ignoring active/reactive power oscillations, the BTB converter output current is

$$i_{m\alpha(p)}^* = \frac{2}{3}\frac{u_\alpha^+ + u_\alpha^-}{[(u_\alpha^+)^2 + (u_\beta^+)^2] + [(u_\alpha^-)^2 + (u_\beta^-)^2]} P_m^*$$
$$i_{m\beta(p)}^* = \frac{2}{3}\frac{u_\beta^+ + u_\beta^-}{[(u_\alpha^+)^2 + (u_\beta^+)^2] + [(u_\alpha^-)^2 + (u_\beta^-)^2]} P_m^*$$
$$i_{m\alpha(q)}^* = \frac{2}{3}\frac{u_\beta^+ + u_\beta^-}{[(u_\alpha^+)^2 + (u_\beta^+)^2] + [(u_\alpha^-)^2 + (u_\beta^-)^2]} Q_m^*$$
$$i_{m\beta(q)}^* = \frac{2}{3}\frac{-u_\alpha^+ - u_\alpha^-}{[(u_\alpha^+)^2 + (u_\beta^+)^2] + [(u_\alpha^-)^2 + (u_\beta^-)^2]} Q_m^* \quad (19)$$

In existing mainstream CCG strategy, the coefficients k_p^+, k_p^-, k_q^+, k_q^- are embedded in (19) to achieve flexible active/reactive current injection [32],

$$i_{m\alpha(p)}^* = \frac{2}{3}\frac{k_p^+ u_\alpha^+ + k_p^- u_\alpha^-}{k_p^+[(u_\alpha^+)^2 + (u_\beta^+)^2] + k_p^-[(u_\alpha^-)^2 + (u_\beta^-)^2]} P_m^*$$
$$i_{m\beta(p)}^* = \frac{2}{3}\frac{k_p^+ u_\beta^+ + k_p^- u_\beta^-}{k_p^+[(u_\alpha^+)^2 + (u_\beta^+)^2] + k_p^-[(u_\alpha^-)^2 + (u_\beta^-)^2]} P_m^*$$
$$i_{m\alpha(q)}^* = \frac{2}{3}\frac{k_q^+ u_\beta^+ + k_q^- u_\beta^-}{k_q^+[(u_\alpha^+)^2 + (u_\beta^+)^2] + k_q^-[(u_\alpha^-)^2 + (u_\beta^-)^2]} Q_m^*$$
$$i_{m\beta(q)}^* = \frac{2}{3}\frac{-k_q^+ u_\alpha^+ - k_q^- u_\alpha^-}{k_q^+[(u_\alpha^+)^2 + (u_\beta^+)^2] + k_q^-[(u_\alpha^-)^2 + (u_\beta^-)^2]} Q_m^* \quad (20)$$

In existing strategy in (20), the network impedance, which has a great influence on the phase angle and amplitude for PCC voltage, has often been overlooked [32]. In order to improve the MG's LVRT ability, a novel CCG strategy is proposed by considering the network impedance as

$$i_{m\alpha(p)}^* = \frac{2}{3}\frac{k_p^+ u_\alpha^+ + k_p^- \dfrac{R_m}{\sqrt{R_m^2 + X_m^2}} u_\alpha^-}{k_p^+[(u_\alpha^+)^2 + (u_\beta^+)^2] + k_p^- \dfrac{R_m}{\sqrt{R_m^2 + X_m^2}}[(u_\alpha^-)^2 + (u_\beta^-)^2]} P_m^*. \quad (21a)$$

$$i_{m\beta(p)}^* = \frac{2}{3}\frac{k_p^+ u_\beta^+ + k_p^- \dfrac{R_m}{\sqrt{R_m^2 + X_m^2}} u_\beta^-}{k_p^+[(u_\alpha^+)^2 + (u_\beta^+)^2] + k_p^- \dfrac{R_m}{\sqrt{R_m^2 + X_m^2}}[(u_\alpha^-)^2 + (u_\beta^-)^2]} P_m^*. \quad (21b)$$

$$i_{m\alpha(q)}^* = \frac{2}{3}\frac{k_q^+ u_\beta^+ + k_q^- \dfrac{X_m}{\sqrt{R_m^2 + X_m^2}} u_\beta^-}{k_q^+[(u_\alpha^+)^2 + (u_\beta^+)^2] + k_q^- \dfrac{X_m}{\sqrt{R_m^2 + X_m^2}}[(u_\alpha^-)^2 + (u_\beta^-)^2]} Q_m^*. \quad (21c)$$

$$i_{m\beta(q)}^* = \frac{2}{3}\frac{-k_q^+ u_\alpha^+ - k_q^- \dfrac{X_m}{\sqrt{R_m^2 + X_m^2}} u_\alpha^-}{k_q^+[(u_\alpha^+)^2 + (u_\beta^+)^2] + k_q^- \dfrac{X_m}{\sqrt{R_m^2 + X_m^2}}[(u_\alpha^-)^2 + (u_\beta^-)^2]} Q_m^*. \quad (21d)$$

To avoid tripping of BTB converter, the peak current limiting in (16) is achieved as

$$\begin{bmatrix} i_{ma}^* \\ i_{mb}^* \\ i_{mc}^* \end{bmatrix} = \frac{I_{\max}}{I_{peak}}\begin{bmatrix} i_{m\alpha(p)}^* + i_{m\alpha(q)}^* \\ -\dfrac{1}{2}(i_{m\alpha(p)}^* + i_{m\alpha(q)}^*) + \dfrac{\sqrt{3}}{2}(i_{m\beta(p)}^* + i_{m\beta(q)}^*) \\ -\dfrac{1}{2}(i_{m\alpha(p)}^* + i_{m\alpha(q)}^*) - \dfrac{\sqrt{3}}{2}(i_{m\beta(p)}^* + i_{m\beta(q)}^*) \end{bmatrix}. \quad (22)$$

Various proportional-integral (PI) control methods and proportional-resonant (PR) control methods have been studied to improve the quality of closed-loop current control [33]-[34]. Generally, there are three reference frames for power electronic control: synchronous reference frame (dq), stationary reference frame ($\alpha\beta$), and natural frame (abc). To achieve zero steady-state current tracking error, the PI control in dq frame is the conventional popular technique to hold an infinite gain for tracking dc reference [33]-[34]. However, it is not well suited for ac reference (e.g., current control in single-phase inverter or three-phase inverter in $\alpha\beta$ frame), due to the steady-state error caused by finite gain [33]-[34]. In addition, the dq frame controller is more complex than the $\alpha\beta$ frame controller, since the significant computational effort is required to realize several transformations from $\alpha\beta$ to dq frame [33]-[34]. A viable alternative to dq frame PI controllers are $\alpha\beta$ frame PR controller, for achieving zero steady-state error tracking of ac reference [33]-[34].

For inverter control, although voltage-controlled (VC) mode is increasing popular, the current-controlled (CC) mode still has many applications [21]-[22], [32] and is more suitable for LVRT/FRT due to the rapid injection ability of reactive current/power. For CC model, the $\alpha\beta$ frame control is widely applied for LVRT/FRT and voltage support [10], [22], [32]. Similar to these previous works [10], [22], [32], in this paper, the inverter is operated at CC model, and the $\alpha\beta$ frame PR controller with acceptable control complexity is adopted to achieve a rapid and direct reactive current/power injection ability with zero steady-state error. On the other hand, an auxiliary universal controller is proposed to achieve transition

between CC and VC mode [10]. Thus, the core essence of AFCL method can also applied to VC mode [10].

D. MSC Control

The MGs generally contain energy storage inside, thus, MGs are regarded as dispatchable power sources. In BTB converter, the GSC injects active/reactive power into the UG based on the requirement of LVRT, while the MSC injects the reference power into the GSC. The function of MSC is to extract the reference power from MGs and maintain the stability of dc voltage (u_{dc}) [27]. The stability of dc voltage is essential for BTB converter, since it plays important role in active power balance between GSC and MSC.

The dc link capacitor current is described as

$$C_{dc}\frac{du_{dc}}{dt} = i_{dc} = i_{MSC} - i_{GSC} .$$ (23)

where i_{MSC}, i_{GSC} are current in MSC and GSC side of dc link.

During normal operation, i_{MSC} and i_{GSC} are equal, and the dc link voltage remains constant. During fault condition, the PCC voltage sags will cause over-voltage across dc link capacitor. In order to stabilize dc voltage, a conventional dc chopper is applied in BTB converter [35]. The dc chopper is activated when dc voltage fluctuates and the resistor (R_{chop}) can dissipate extra energy flowing to protect chopper converter from damage. The chopper converter switch is triggered based on dc link voltage [35]. The duty cycle of dc chopper switch is described as

$$D = \frac{R_{chop}}{u_{dc}^2}(P_{MSC} - P_{GSC}) .$$ (24)

where P_{MSC} and P_{GSC} are the active power in MSC and GSC side of dc link, and their reference value is P_m^*.

Based on (23)-(24) and considering the stability control of dc voltage, the MSC power injection and the dc chopper action is carried out, which is detailed in Fig. 4.

E. Design of Adjustable Coefficients

1) Design for LVRT

The key to LVRT operation relies on the effective execution of the grid code requirement, which needs the precise coefficients design in (3)-(4). Considering PCC voltage amplitude compensation, the reference of positive/negative sequence reactive current in (3)-(4) is described as

$$I_{mq}^{+*} = \frac{X_m}{\sqrt{R_m^2 + X_m^2}}(U^{+*} - U_F^+) .$$ (25)

$$I_{mq}^{-*} = \frac{-X_m}{\sqrt{R_m^2 + X_m^2}}(-U_F^-) .$$ (26)

Divide (25) and (26) by (3) and (4), the coefficients for the grid code requirement are obtained as

$$k_{LVRT}^+ = \frac{X_m}{\sqrt{R_m^2 + X_m^2}}\frac{U^{+*} - U_F^+}{U_N - U_F^+}\frac{U_N}{I_N} .$$ (27)

$$k_{LVRT}^- = \frac{-X_m}{\sqrt{R_m^2 + X_m^2}}\frac{-U_F^-}{U_N - U_F^-}\frac{U_N}{I_N} .$$ (28)

2) Design for AFCL

The key of the AFCL method relies on effective control for the active/reactive current injection of BTB converter. In order to fit the PAA function to relieve the impact of MGs fault current on system fault current, the coefficients for CCG strategy in (21) are constrained as

$$I^{+*} = \sqrt{\left[\frac{k_p^+ U^+ P_m^*}{k_p^+(U^+)^2 + k_p^-\frac{R_m}{\sqrt{R_m^2+X_m^2}}(U^-)^2}\right]^2 + \left[\frac{k_q^+ U^+ Q_m^*}{k_p^+(U^+)^2 + k_q^-\frac{X_m}{\sqrt{R_m^2+X_m^2}}(U^-)^2}\right]^2} = \frac{I_{mq}^{+*}}{\sin(\theta_m^+)}$$ (29a)

$$I^{-*} = \sqrt{\left[\frac{k_q^-\frac{R_m}{\sqrt{R_m^2+X_m^2}}U^- P_m^*}{k_p^+(U^+)^2 + k_p^-\frac{R_m}{\sqrt{R_m^2+X_m^2}}(U^-)^2}\right]^2 + \left[\frac{k_q^-\frac{X_m}{\sqrt{R_m^2+X_m^2}}U^- Q_m^*}{k_p^+(U^+)^2 + k_q^-\frac{X_m}{\sqrt{R_m^2+X_m^2}}(U^-)^2}\right]^2} = \frac{I_{mq}^{-*}}{\sin(\theta_m^-)}$$ (29b)

$$\tan(\theta_m^+) = \frac{Q_m^+}{P_m^+} = \frac{k_p^+(U^+)^2 + k_p^-\frac{R_m}{\sqrt{R_m^2+X_m^2}}(U^-)^2}{k_q^+(U^+)^2 + k_q^-\frac{X_m}{\sqrt{R_m^2+X_m^2}}(U^-)^2}\frac{k_q^+}{k_p^+}\frac{Q_m^*}{P_m^*} .$$ (29c)

$$\tan(\theta_m^-) = \frac{Q_m^-}{P_m^-} = \frac{k_p^+(U^+)^2 + k_p^-\frac{R_m}{\sqrt{R_m^2+X_m^2}}(U^-)^2}{k_q^+(U^+)^2 + k_q^-\frac{X_m}{\sqrt{R_m^2+X_m^2}}(U^-)^2}\frac{k_q^- X_m}{k_p^- R_m}\frac{Q_m^*}{P_m^*} .$$ (29d)

Based on (29), the k_q^+, k_q^-, k_p^+, k_p^- are designed as

$$k_q^+ = \frac{I_{mq}^{+*}}{U^+}, \qquad k_q^- = \frac{I_{mq}^{-*}\sqrt{R_m^2+X_m^2}}{U^- X_m}$$

$$k_p^+ = \frac{I_{mp}^{+*}}{U^+}, \qquad k_p^- = \frac{I_{mp}^{-*}\sqrt{R_m^2+X_m^2}}{U^- R_m} .$$ (30)

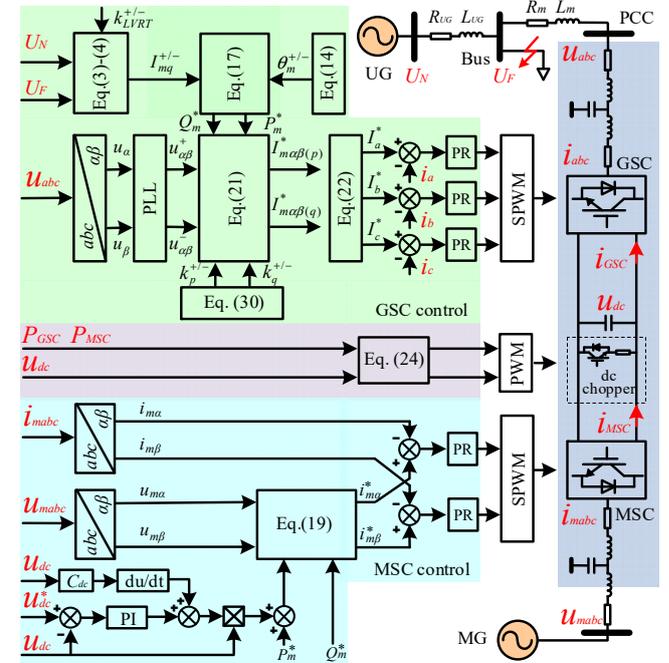### F. AFCL Method for the LVRT of Networked MGs

Fig. 4. The LVRT of networked MGs with BTB converter.

According to the analyses of Section III.A-E, the LVRT of networked MGs is combined with GSC control and MSC control. In GSC, the AFCL consists of PAA, CI, and CCG

strategies to relieve the impact of MGs fault current. The LVRT of networked MGs with BTB converter is illustrated in Fig. 4. The red variable is the sampling and input signals.

IV. CASE STUDY

A. System Data

The effectiveness of the proposed AFCL method for the LVRT of networked MGs is validated based on Matlab/Simulink. For the sake of analysis, the networked MGs consist of two MGs with the same capacity and network impedance. The performance of the proposed AFCL method is tested with three-phase unbalanced voltage sag, as shown in Fig. 5. The fault occurs at 0.05s and is cleared at 0.20s. The system and control parameters are given in Tables I and II, respectively.
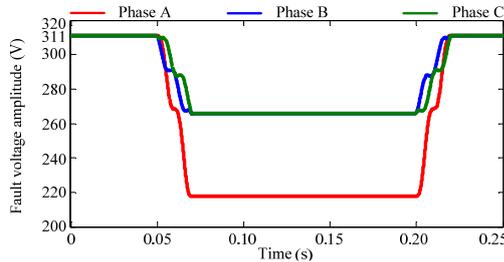

Fig. 5. The fault voltage amplitude of fault bus.

TABLE I. THE SYSTEM NETWORK PARAMETERS

Parameters	Symbol	Value	Unit
Network impedance of UG	R_{UG} / L_{UG}	0.2 / 1	Ω / mH
Network impedance of GSC for MG#1	R_1 / L_1	1.5 / 3	Ω / mH
Network impedance of GSC for MG#2	R_2 / L_2	1.5 / 3	Ω / mH
DC capacitor	C_{dc}	40	μF
GSC side impedance of LCL filter	R / L	0.01 / 2.5	Ω / mH
MSC side impedance of LCL filter	R / L	0.01 / 0.5	Ω / mH
Capacitor of LCL filter	C_{filter}	40	μF
UG nominal voltage	U_g	311	V
DC voltage	u_{dc}	800	V
Resistance of dc chopper	R_{chop}	1.5	Ω
Nominal frequency	f	50	Hz
Cutoff angular frequency	ω_c	70	rad/s
Switching frequency	f_s	10	kHz

TABLE II. THE CONTROL PARAMETERS

Parameters	Symbol	Value
Grid code coefficients with existing FCL [2]	k^+_{LVRT} / k^-_{LVRT}	2.2 / 3
Grid code coefficients with proposed AFCL	k^+_{LVRT} / k^-_{LVRT}	2.5 / 3.5
Adjustable coefficients with existing FCL [23]-[25]	k^+_p / k^-_p	-0.08 / -0.7
	k^+_q / k^-_q	-0.04 / 12
Adjustable coefficients with proposed AFCL	k^+_p / k^-_p	0.1 / -0.8
	k^+_q / k^-_q	0.04 / 6

B. PAA Strategy

Taking positive sequence component as an example, the phase angles of MGs fault current is shown in Fig. 6.

The phase angles of MG#1 and MG#2 fault currents are almost consistent, since the capacity and network impedance of MGs are set as the same. In the case without PAA strategy [2]-[3], the phase angle is the smallest since the current only needs to execute the normal LVRT operation. In the case with PAA strategy [23]-[25], the phase angle is larger than that in the case without PAA, since an extra phase angle is needed in order to relieve the impact of MGs fault current. Besides, the phase angle in the case with proposed PAA is larger than that

with existing PAA [23]-[25], since the phase angle in proposed PAA is updated and shifted with a more precise value by further considering the voltage's phase angle difference from UG to fault branch and from MGs to fault branch.
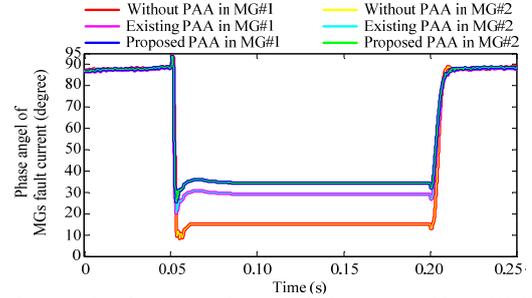

Fig. 6. Phase angle of MG#1 and MG#2 fault current without [2]-[3], with existing [23]-[25] and with proposed PAA strategy.

C. CCG Strategy

The coefficients (k^-_p and k^-_q) are tested and verified to illustrate the effectiveness of the proposed CCG strategy in (21), which considers the characteristics of output current and network impedance together. As shown in Fig. 7, compared with [22], [32], it is evident that the proposed CCG strategy is more helpful for the recovery of positive sequence voltage and the reduction of negative sequence voltage. Therefore, the proposed CCG strategy can improve the voltage support ability during the LVRT of networked MGs under fault conditions.
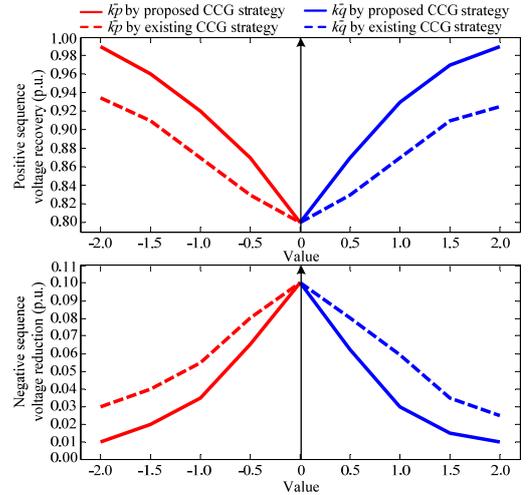

Fig. 7. Comparison of proposed and existing CCG strategy in [22], [32].

D. AFCL Method for LVRT of Networked MGs

The LVRT of networked MGs is tested based on the UG fault voltage in Fig. 5. In order to keep the networked MGs stay in the grid-connected state, the PCC voltage should be supported, as shown in Figs. 8-9. As can be seen, under the same fault, both existing and proposed method can support the PCC voltage to the rated value within the allowable error. The proposed AFCL method has a better voltage recovery ability during LVRT operation, and can support PCC voltage more balanced and has less fluctuation. This is mutually corroborated with the proposed CCG strategy in the analyses of Fig.7. During LVRT, the MGs fault currents with existing and proposed AFCL are shown in Figs. 10-11. As can be seen, once UG fault occurs, the phase angle and amplitude of MG#1 and
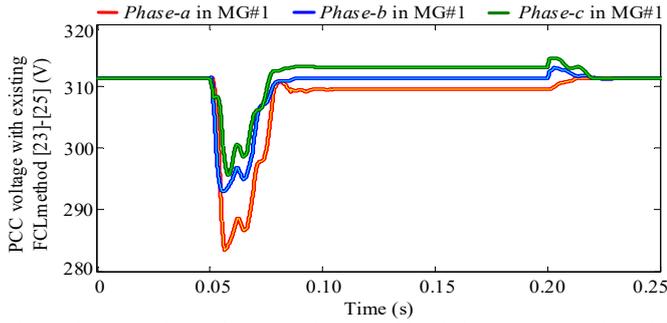
Fig. 8. The PCC voltage of MG#1 and MG#2 with existing FCL method in [23]-[25].
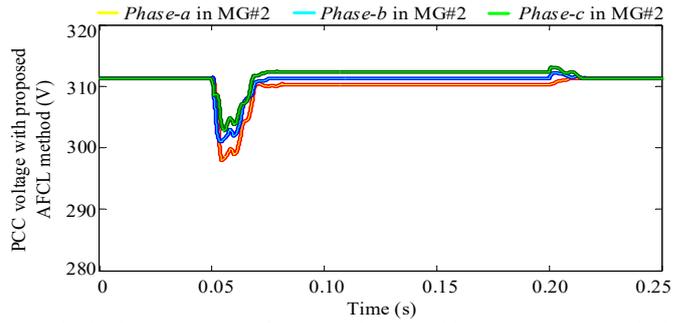
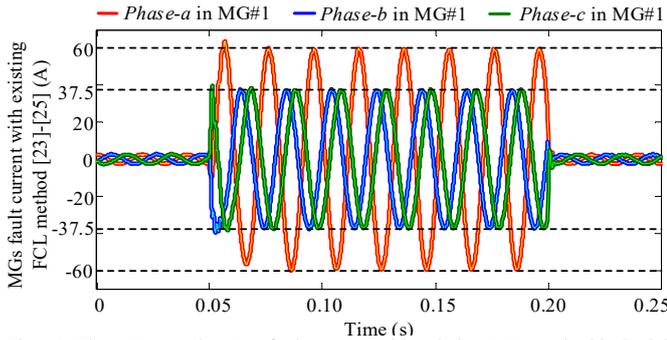Fig. 9. The PCC voltage of MG#1 and MG#2 with proposed AFCL method.

Fig. 10. The MG#1 and MG#2 fault current with existing FCL method in [23]-[25].
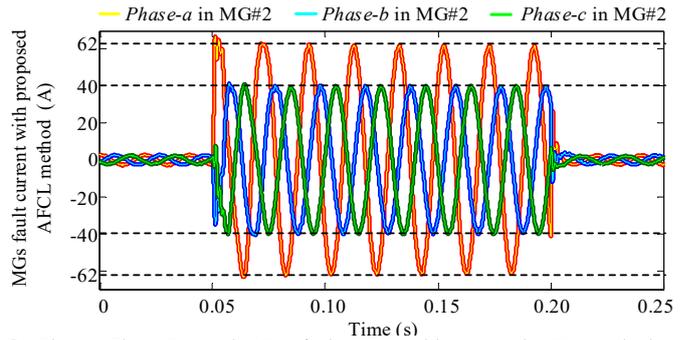
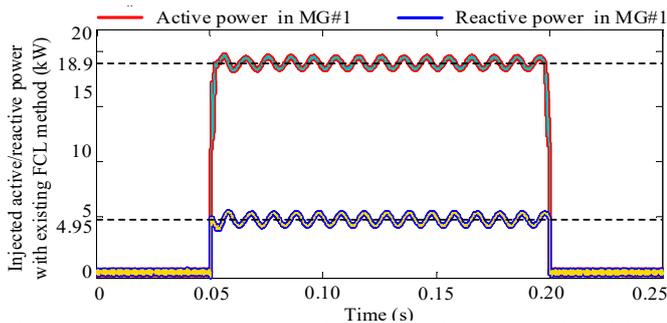Fig. 11. The MG#1 and MG#2 fault current with proposed AFCL method.

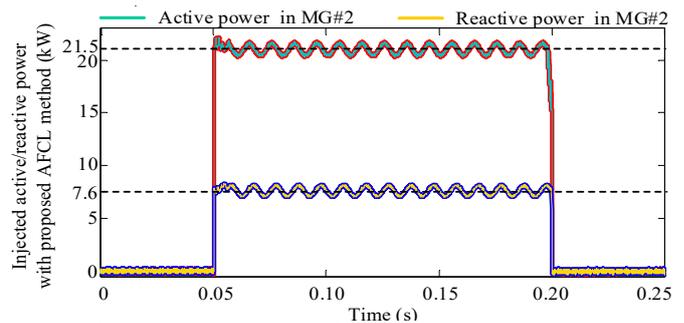Fig. 12. The MG#1 and MG#2 power injected by existing method in [23]-[25].

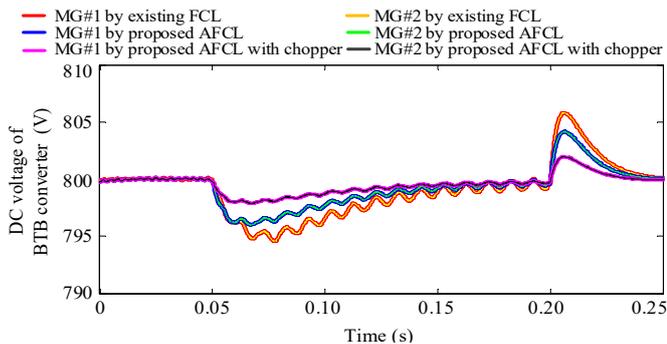Fig. 13. The MG#1 and MG#2 power injected by proposed AFCL method.

Fig. 14. DC voltage of BTB converter with proposed/existing FCL in [23]-[25].
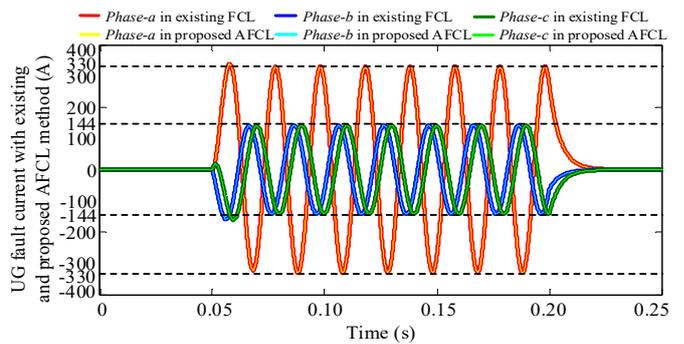
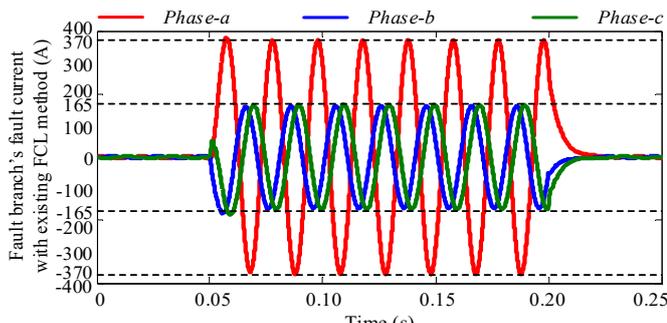Fig. 15. The UG fault current with proposed/existing FCL in [23]-[25].

Fig. 16. The system fault current with existing FCL method in [23]-[25].
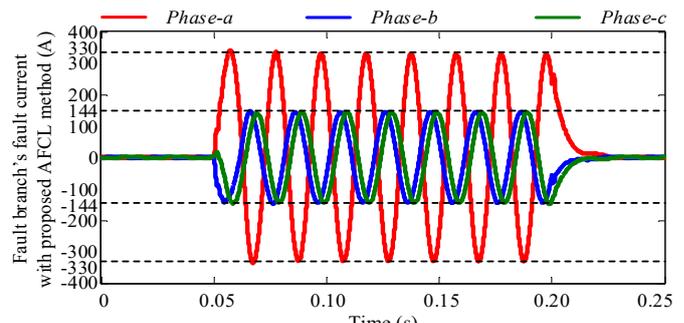
Fig. 17. The system fault current with proposed AFCL method.

MG#2 fault currents are different due to the different phase angle adjusted by PAA in Fig. 6. With considering voltage's phase angle differences from UG to fault branch and MGs to fault branch, the MGs fault current in the case with existing FCL [23]-[25] lags that with proposed AFCL. The power injections for the LVRT of networked MGs with existing and proposed AFCL are shown in Figs. 12-13. The active/reactive power is injected by MG#1 and MG#2 with different phase angles. Due to the presence of PAA, the amount of active/reactive power would be much larger than it is in cases with existing FCL for the same goal of PCC voltage support.

The dc voltage of BTB converter with existing and proposed AFCL is shown in Fig. 14. The u_{dc} is stabilized at a reference value, 800V, which is helpful for the active power flow between GSC and MSC. When considering dc chopper, the dc voltage is more stable by proposed AFCL method. The u_{dc} has fluctuation during LVRT operation. The active power fluctuation in Figs. 12-13 is also corroborated by the fluctuation of u_{dc}.

The UG fault current under the condition of existing FCL and proposed AFCL is shown in Fig. 15. The UG fault current with existing and proposed AFCL is almost the same because the fault bus voltage is almost the same in these two cases.

The system fault currents with existing and proposed AFCL are shown in Figs. 16-17 and Table III. The system fault current is the sum of UG and MGs fault current. It can be found that the amplitude/angle of system fault current with existing FCL and proposed AFCL are different. In the case with existing FCL, the amplitude of system fault current is larger than UG fault current. In the case with proposed AFCL, the amplitude of system fault current is almost the same as in UG fault current. These results are also summarized in Table III. In the existing FCL without (with) existing PAA strategy, the MG#1 and MG#2 can contribute 48 A (40 A), 25 A (21 A) and 25 A (21 A) to system fault current in *phase-a*, *phase-b*, and *phase-c*, respectively. In the proposed AFCL method, the MG#1 and MG#2 will not contribute fault current to system. The fault current contribution rate, which refers to the ratio of system fault current increments to MG output fault current, is also analyzed in Table IV. Therefore, based on the proposed AFCL, the MGs fault current is more effectively relieved and has no influence ($\approx$0% contribution) on system fault current.

TABLE III. COMPARISON OF EXISTING AND PROPOSED AFCL

Fault current	Phase-a	Phase-b	Phase-c
UG fault current (A)	330	144	144
MG#1 and MG#2 fault current by existing FCL without PAA [2], [21]-[22] (A)	55 / 55	35.2 / 35.2	35.2 / 35.2
MG#1 and MG#2 fault current by existing FCL with existing PAA [23]-[25] (A)	60 / 60	37.5 / 37.5	37.5 / 37.5
MG#1 and MG#2 fault current by proposed AFCL (A)	62 / 62	40 / 40	40 / 40
System fault current by existing FCL without PAA [2], [21]-[22]	378	169	169
System fault current by existing FCL with existing PAA [23]-[25]	370	165	165
System fault current by proposed AFCL (A)	$\approx$330	$\approx$144	$\approx$144

TABLE IV. CONTRIBUTION ANALYSES OF EXISTING AND PROPOSED AFCL

Fault current	Phase-a	Phase-b	Phase-c
MG#1 and MG#2 fault current contribution rate by existing FCL without PAA [2], [21]-[22]	87.3%	71%	71%
MG#1 and MG#2 fault current contribution rate by existing FCL with existing PAA [23]-[25]	66.7%	56%	56%
MG#1 and MG#2 fault current contribution rate by proposed AFCL	$\approx$ 0%	$\approx$ 0%	$\approx$ 0%

E. Multiple Operation Performance Analyses

The operation performances of existing and proposed method are compared in Fig. 18. During pre- and post- fault conditions, both unbalanced voltage factor (UVF) and relative error of phase voltage are similar due to the normal operation. During fault condition, in Fig. 18(a), the UVF of PCC voltage supported by proposed method is lower than that by existing method, which verifies a stronger voltage support ability of proposed method. In Fig. 18(b)-(d), the relative error of PCC phase-*abc* voltage supported by proposed method is also lower than that by existing method. These can further indicate that the proposed method can make voltage more balance and precise. Although the maximum UVF and relative error are within allowable error by 2% and 8% respectively, the proposed method provides a better performance.
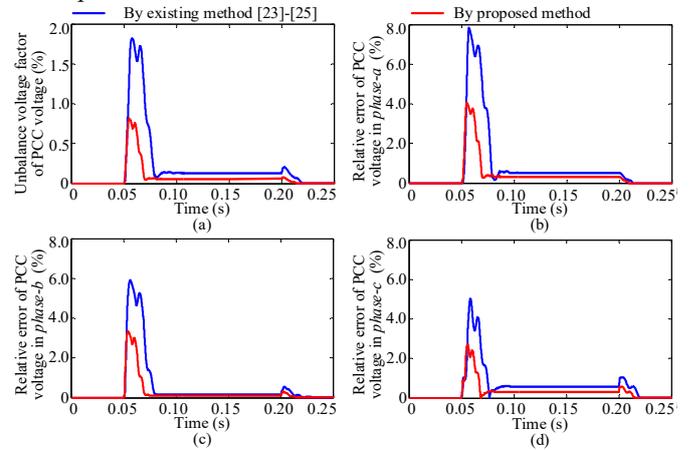

Fig. 18. Performance comparison of existing [23]-[25] and proposed method: (a) UVF and (b)-(d) relative errors of PCC voltage in *phase-a*, *phase-b*, and *phase-c*, respectively.

In order to further verify the effective of proposed AFCL method, the system is tested with different voltage sag depths, which is shown in Fig. 19. The PCC fault voltage ranges from 10%~100%. On the basis of LVRT, the MGs output fault current is the core concern in our proposed method. Taking MG#1's *phase-a* current as an example, the larger the voltage drops, the larger the output fault current is. In addition, the MG fault current injected by proposed method is larger than existing method [23]-[25], because a more precise leading phase angle of current will require a larger amplitude of current for the goal of LVRT. This rule is also verified in the analysis of Figs. 10-13.
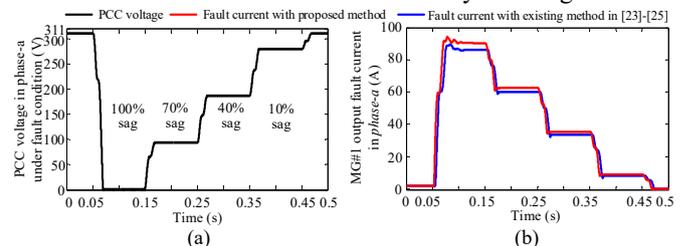

Fig. 19. Comparison of different fault sag depths: (a) PCC fault voltage, (b) the MG#1 output fault current in *phase-a* injected by existing [23]-[25] and proposed method.

F. Time Delay Analysis

The impact of communication time delay on the amplitude of system fault current in *phase-a* is shown in Fig. 20. When there

is no time delay, the AFCL can be activated immediately. Otherwise, the execution of AFCL is delayed after fault information data is received. During the delay period, the system fault current is larger than UG fault current. After the delay, the system fault current is almost the same to UG fault current, and the system fault current increasing problem is solved. The length of time delay does not influence the nature of AFCL method. In practice, the AFCL is activated once the time delay ends. During communication delay period, the LVRT can be first conducted by traditional method in the MG local controller once PCC voltage drops below 0.9 p.u. Then, when the remote UG fault information data are transmitted to the MG local controller, the AFCL strategy can be operated to relieve the impact of MG fault current on system fault current.
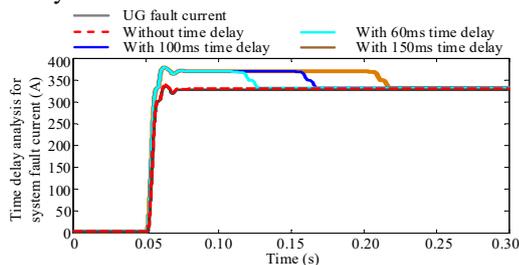

Fig. 20. Time delay analysis for system fault current amplitude in *phase-a*.

G. Additional Discussions and Analyses

1) Practical application of proposed method

a) In terms of fault location: The main contribution of proposed AFCL is the novel PAA strategy, which considers the practical voltage's phase angle differences from UG to fault branch and from MGs to fault branch. In practical system, it is important to know fault branch location, in order to determine the precise voltage's phase angle differences. Fortunately, there are many relatively mature technologies to know fault branch and amplitude/phase angle of voltage/current and the phase angle differences, according to the equipped sensors, GPS-based MPUs, intelligent electronic devices (IEDs) and phasor data concentrators (PDCs), *et al* [36]-[37]. The real-time synchronized phasor (phase angle) data and synchronized voltage/current waveform data provided by PMUs and IEDs are helpful for power system supervision and the protection relay applications including fault location [36]-[37]. Numerous PMU-based fault location techniques or algorithms for two- or three- terminal homogeneous or nonhomogeneous lines have been proposed in [36]-[37]. The fault location can be determined based on three-phase currents/voltages which is sampled from the bus equipped with fault locators or sensor detection devices [36]. In addition, the sampling rate has reduced from 20 kHz to 1 kHz, and the detecting time of fault location has reduced to less than 7 ms in two-terminal lines system [37]. On the one hand, our paper mainly focuses on the AFCL to keep system fault current amplitude unchanged, rather than a specific fault location determination method. On the other hand, there are many ready-made and state-of-the-art technologies for fault location, which provide significant support of practical application of proposed AFCL method. Therefore, the proposed AFCL method can be applied to the actual power systems.

b) In terms of network impedance: In practical power system, the network impedance is important for the proposed CCG strategy. This network impedance is variable for different faults. Fortunately, the determination of network impedance between different node is already a very mature technology, which has been widely calculated in [38]. These ready-made technologies can also support the practical application of proposed CCG strategy in AFCL.

c) In terms of hardware: 1) Sensors and PMUs are needed to detect the amplitude/phase angle of UG/MG fault current/voltage, and the phase angle differences; 2) The related communication lines are required for the transmission of fault information data; 3) Converters need more input/output (I/O) interface to receive the fault information data from UG; 4) To relieve MG fault currents, the PAA module is required in inverter controller for phase angle calculation; 5) The CI module is also required in inverter controller to match the PAA function for LVRT.

2) Improvements of proposed method

According to the modeling, mathematical analyses, parameter designs, and multiple scenarios analyses, the proposed method provides the following improvements,

a) Suitable for applications with more stricter power quality. Compared with [2], [22], [23]-[25], due to the BTB converter application, the proposed method is more suitable for industrial distribution networks with a large proportion of sensitive loads, such as chemical plants and semiconductor devices. The proposed method can be also applied to other devices, such as wind and photovoltaic inverter, AC/DC microgrids, and HVDC.

b) System fault current increasing challenge is solved more thoroughly. More than just focusing on inverter protection by peak current limiting [2], [21]-[22], a novel PAA strategy is proposed to avoid the increasing of system fault current by relieving the contribution of MG fault current on system fault current. Compared with [23]-[25], the adjusted phase angle of MG fault current is more precise by considering the voltage's phase angle differences from UG to fault branch and from MGs to fault branch. The existing methods will inevitably increase system fault current [2], [21]-[22], [23]-[25], while the proposed method can keep the system fault current level unchanged.

c) LVRT performance is improved. Compared with [22], [32], by directly embedding network impedance characteristics, the proposed CCG strategy is more helpful for positive sequence voltage recovery and negative sequence voltage reduction, and the UVF and relative error of PCC voltage is lower, leading to a better voltage support performance for LVRT of MGs.

d) Further reduce reliance on protective equipment. Compared with [17]-[18], the system fault current limitation will not need to install additional protection devices, such as fault current limiters [17]-[18], since system fault current amplitude is kept unchanged by proposed AFCL method.

e) Further reduce reliance on relay protection. Compared with [2], [21]-[22], the relay protections (e.g., over-current amplitude protection and coordination control between primary and secondary protection) will be disturbed, since system fault current will increase with the penetration of MGs. Based on the

proposed AFCL method, the relay protection devices do not need to be updated even if the MGs are integrated in the future.

f) Time delay is analyzed. Compared with [2], [21]-[22], [23]-[25], the communication time delay is considered during fault current limitation.

V. CONCLUSION

Under the UG fault condition, in view of the high-level system fault current during the LVRT of networked MGs, an AFCL method is proposed to avoid monotonically increasing system fault currents during the LVRT of networked MGs. In this method, in order to improve the voltage control ability of LVRT, the CCG strategy is proposed by embedding the network impedance characteristics. Then, in order to achieve a better fault current limitation by relieving the impact of MGs fault current, the PAA strategy is proposed with considering voltage's phase angle difference from UG and MGs to fault branch. Meanwhile, the CI strategy is conducted to fit the feature of PAA. Numerous simulation results have validated the improvements of the proposed AFCL method with a successful LVRT, meanwhile, the networked MGs fault current does not increase the system fault current amplitude.

Considering the fields with a high proportion of sensitive load, the BTB converter is widely used for the PCC connection point of DGs and MGs to provide high power quality. To reduce the fault current level, the AFCL method can be applied to the BTB converter, and can be also used to the other inverter products, such as wind and photovoltaic inverter, AC/DC microgrids, and HVDC transmission system.

VI. REFERENCES

[1] Q. Zhou, M. Shahidehpour, et al, "Distributed Control and Communication Strategies in Networked Microgrids," *IEEE Communications Surveys & Tutorials*, vol. 22, no. 4, pp. 2586-2633, Fourth quarter 2020.

[2] X. Zhao, J. M. Guerrero, et al, "Low-Voltage Ride-Through Operation of Power Converters in Grid-Interactive Microgrids by Using Negative-Sequence Droop Control," *IEEE Trans. Power Electron.*, vol. 32, no. 4, pp. 3128–3142, April 2017.

[3] I. Sadeghkhani, M. E. H. Golshan, A. Mehrizi-Sani, J. M. Guerrero, "Low-voltage ride-through of a droop-based three-phase four-wire grid-connected microgrid," *IET Gener. Transm. Distrib.*, vol. 12, no. 8, pp. 1906–1914, 2018.

[4] Y. He, M. Wang and Z. Xu, "Coordinative Low-Voltage-Ride-Through Control for the Wind-Photovoltaic Hybrid Generation System," *IEEE Journal of Emerging & Selected Topics in Power Electronics*, vol. 8, no. 2, pp. 1503–1514, Jun. 2020.

[5] Y. Yang, F. Blaabjerg, and Z. Zou, "Benchmarking of grid fault modes in single-phase grid-connected photovoltaic systems," *IEEE Trans. Ind. Appl.*, vol. 49, no. 5, pp. 2167–2176, Sep./Oct. 2013.

[6] N. Jelani and M. Molinas, "Asymmetrical fault ride through as ancillary service by constant power loads in grid-connected wind farm," *IEEE Trans. Power Electron.*, vol. 30, no. 3, pp. 1704–1713, Mar. 2015.

[7] P. P. Vergara, J. M. Rey, H. R. Shaker, J. M. Guerrero, *et al*, "Distributed Strategy for Optimal Dispatch of Unbalanced Three-Phase Islanded Microgrids," *IEEE Trans. Smart Grid*, vol. PP, no. 99, pp. 1-15, 2018.

[8] A. Micallef, M. Apap, and J. M. Guerrero, "Singlephase microgrid with seamless transition capabilities between modes of operation," *IEEE Trans. Smart Grid*, vol. 6, no. 6, pp. 2736–2745, Nov. 2015.

[9] J. Chan, J. Milanovic, and A. Delahunty, "Generic failure-risk assessment of industrial processes due to voltage sags," *IEEE Trans. Power Del.*, vol. 24, no. 4, pp. 2405–2414, Oct. 2009.

[10] P. Prasanna, E. Mohammad, K. G. Masoud, A. K. Sayed, "Fault Ride-Through Capability of Voltage-Controlled Inverters," *IEEE Transactions on Ind. Electron.*, vol. 65, no. 10, pp. 7933-7943, Oct. 2018.

[11] J. A. Laghari, H. Mokhlis, M. Karimi, A. H. A. Bakar, and H. Mohamad, "Computational intelligence based techniques for islanding detection of distributed generation in distribution network: A review," *Energy Convers. Manag.*, vol. 88, pp. 139–152, Dec. 2014.

[12] W. Wan, M. A. Bragin, B. Yan, Y. Qin, et al, "Distributed and Asynchronous Active Fault Management for Networked Microgrids," *IEEE Trans. Power System*, vol. 35, no. 5, pp. 3857-3868, Sep. 2020.

[13] A. Camacho, M. Castilla, J. Miret, L. G. de Vicuña, and R. Guzman, "Positive and negative sequence control strategies to maximize the voltage support in resistive–inductive grids during grid faults," *IEEE Trans. Power Electron.*, vol. 33, no. 6, pp. 5362–5373, Jun. 2018.

[14] W.F. Wan, Y. Li, B. Yan, *et al.*, "Active Fault Management for Microgrids," Annual Conference of the IEEE Industrial Electronics Society (IECON), pp. 1-6, 2018.

[15] S. A. Gopalan, V. Sreeram, H. H.C.Iu, "A review of coordination strategies and protection schemes for microgrids," *Renewable and Sustainable Energy Reviews*, vol. 32, pp. 222-228, April 2014.

[16] R. Li, L. Xu, Y. Yao, "DC Fault Detection and Location in Meshed Multiterminal HVDC Systems Based on DC Reactor Voltage Change Rate," *IEEE Trans. Power Del.*, vol. 32, no. 3, pp. 1516–1526, June. 2017.

[17] M. A. Zamani, T. S. Sidhu, and A. Yazdani, "A protection strategy and microprocessor-based relay for low-voltage microgrids," *IEEE Trans. Power Del.*, vol. 26, no. 3, pp. 1873–1883, July 2011.

[18] E. Sortomme, S. S. Venkata, and J. Mitra, "Microgrid protection using communication-assisted digital relays," *IEEE Trans. Power Del.*, vol. 25, no. 4, pp. 2789–2796, Oct. 2010.

[19] H. Nourmohamadi, M. Nazari-Heris, M. Sabahi, M. Abapour, "A Novel Structure for Bridge-Type Fault Current Limiter: Capacitor-Based Nonsuperconducting FCL," *IEEE Trans. Power Electron.*, vol. 33, no. 4, pp. 3044-3051, 2018.

[20] IEEE Standard for Interconnecting Distributed Resources With Electric Power Systems, IEEE Standard 1547, 2003.

[21] B. Mahamedi, M. Eskandari, J. E. Fletcher, and J. Zhu, "Sequence-Based Control Strategy with Current Limiting for the Fault Ride-Through of Inverter-Interfaced Distributed Generators," *IEEE Trans. Sustainable Energy*, vol. PP, no. 99, pp. 1-10, Dec 2018.

[22] X. Guo, W. Liu and Z. Lu, "Flexible Power Regulation and Current-limited Control of Grid-connected Inverter under Unbalanced Grid Voltage Faults," *IEEE Trans. Power Electron.*, vol. 64, no. 9, pp. 7425–7432, 2017.

[23] N. Rajaei, M. H. Ahmed, M. M. A. Salama, and R. K. Varma, "Fault current management using inverter-based distributed generators in smart grids," *IEEE Trans. Smart Grid*, vol. 5, no. 5, pp. 2183–2193, Sep. 2014.

[24] N. Rajaei and M. M. A. Salama, "Management of fault current contribution of synchronous DGs using inverter-based DGs," *IEEE Trans. Smart Grid*, vol. 6, no. 6, pp. 3073–3081, Nov. 2015.

[25] W. Kou and D. Wei, "Fault ride through strategy of inverter-interfaced microgrids embedded in distributed network considering fault current management," *Sustain. Energy Grids Netw.*, vol. 15, pp. 43–52, Sep. 2018.

[26] E. O. Daniel, M. S. Ali, H. E. Amir, A. C. Claudio, et al, "Trends in Microgrid Control," *IEEE Trans. Smart Grid*, vol. 5, no. 4, pp. 1905-1919, July. 2014.

[27] R. Majumder, A. Ghosh, G. Ledwich, F. Zare, "Power Management and Power Flow Control With Back-to-Back Converters in a Utility Connected Microgrid," *IEEE Trans. Power System*, vol. 25, no. 2, pp. 821-834, 2015.

[28] X. Chen, Y. Zhang, S. Wang, J. Chen, C. Gong, "Virtual-Impedance-Based Control for Voltage-Source and Current-Source Converters," *IEEE Trans. Power Electron.*, vol. 30, no. 12, pp. 7019–7037, Dec. 2015.

[29] X. Wang, Y. Li, F. Blaabjerg, P. Loh, "Impedance-Phased Dynamic Control Method for Grid-Connected Inverters in a Weak Grid," *IEEE Trans. Power Electron.*, vol. 32, no. 1, pp. 274–283, Jan. 2017.

[30] P. Sreekumar and V. Khadkikar, "Direct Control of the Inverter Impedance to Achieve Controllable Harmonic Sharing in the Islanded Microgrid," *IEEE Trans. on Ind. Electron.*, vol. 64, no. 1, pp. 827-837, Jan 2017.

[31] S. Chaudhary, R. Teodorescu, D. Rizadis, L. Mathe, "Low voltage fault ride through control in MMC-HVDC," *IEEE International Symposium on Industrial Electronics*, pp. 750-755, June. 2017.

[32] J. L. Sosa, M. Castilla, J. Miret, "Control Strategy to Maximize the Power Capability of PV Three-Phase Inverters During Voltage Sags," *IEEE Trans. Power Electron.*, vol. 31, no. 4, pp. 3314-3323, April. 2016.

[33] C. Zou, B. Liu, S. D, R. Li, "Stationary Frame Equivalent Model of Proportional-Integral Controller in dq Synchronous Frame," *IEEE Trans. Power Electron.*, vol. 29, no. 9, pp. 4461–4465, Sep. 2014.

[34] A. Kuperman, "Proportional-Resonant Current Controllers Design Based on Desired Transient Performance," *IEEE Trans. Power Electron.*, vol. 30, no. 10, pp. 5341–5345, Oct. 2015.

[35] P. Debre, R. Juneja, D. R. Tutakane, M. R. Ramteke, "Overvoltage protection scheme for back to back converter of grid connected DFIG," *IEEE Industrial Electronics Society (IECON)*, pp. 1-4, Nov. 2015.

[36] Y. Lee, T. Lin, C. Liu, "Multi-Terminal Nonhomogeneous Transmission Line Fault Location Utilizing Synchronized Data," *IEEE Trans. Power Del.*, vol. 34, no. 3, pp. 1030–1038, June 2019.

[37] T. Lin, P. Lin, C. Liu, "An algorithm for locating faults in three-terminal multisection nonhomogeneous transmission lines using synchrophasor measurements," *IEEE Trans. Smart Grid.*, vol. 5, no. 1, pp. 38–50, 2014.

[38] S. Das, S. N. Ananthan, and S. Santoso, "Estimating zero-sequence impedance of three-terminal transmission line and Thevenin impedance using relay measurement data," *Protect. Control Mod. Power Syst.*, vol. 3, pp. 1–10, Dec. 2018.

BIOGRAPHIES

Xubin Liu (M'19) received the B.E. degree in automation from the College of Electrical Engineering in Northwest University for Nationalities, Lanzhou, China in 2013, and the Ph.D. degree in electrical engineering from Hunan University, Changsha, China in 2019.

He is currently a Postdoctoral Researcher with the School of Electrical and Electronic Engineering, Huazhong University of Science and Technology (HUST), Wuhan 430074, China. His research interests include fault ride-through, fault voltage support, fault current limitation, frequency regulation, self-healing control, power electronics control, and energy management system of smart grid.

Xinyu Chen (M'14) received the B.S. and Ph.D. degrees in electrical engineering from Tsinghua University, Beijing, China, in 2009 and 2014, respectively. He was an exchange Ph.D. student at Harvard University, Cambridge, MA, USA, in 2012.

From 2015 to 2016, he was a Postdoctoral Researcher with Harvard University. Since 2016, he has been a Lecturer with Harvard University. He is currently a Professor with the School of Electrical and Electronic Engineering, Huazhong University of Science and Technology (HUST), Wuhan 430074, China. His research interests include power system operation and planning, multi-energy system optimization, renewable energy integration, and energy policy.

Mohammad Shahidehpour (F'01) received the Honorary Doctorate degree from the Polytechnic University of Bucharest, Bucharest, Romania. He is a University Distinguished Professor, the Bodine Chair Professor, and the Director of the Robert W. Galvin Center for Electricity Innovation, Illinois Institute of Technology. He is also with the Center of Research Excellence in Renewable Energy and Power Systems, King Abdulaziz University, Jeddah 2589, Saudi Arabia. He is a fellow of the American Association for the Advancement of Science and the National Academy of Inventors. He is also a member of the U.S. National Academy of Engineering.

Canbing Li (M'06-SM'13) received the B.E. and Ph.D. degree from Tsinghua University, Beijing, China, in 2001 and 2006, respectively, both in electrical engineering.

He is currently a Professor with Shanghai Jiao Tong University, Shanghai, China. His research interests include power systems, smart grid, renewable energy, with an emphasis on large-scale power system dispatch, economic and secure operation of power systems, energy efficiency and energy saving in smart grid, electric demand management of data centers, vehicle-to-grid technologies.

Xia Chen (M'13-SM'18) received the B.S. degree in power system and its automaton from Wuhan University of Technology, China, in 2006, and the M.S. and Ph.D. degrees in electrical engineering from Huazhong University of Science and Technology (HUST), China, in 2008 and 2012, respectively. She was a Post-Doctoral Research Fellow with the University of Hong Kong, from 2012 to 2015. In 2015 she joined the HUST and now she is an associate professor with the School of Electrical and Electronic Engineering, HUST. Her research interests include distributed control technology in microgrid, renewable energy integration technologies, and new smart grid device.

Jinyu Wen (M'10) received the B.S. and Ph.D. degrees in electrical engineering from Huazhong University of Science and Technology (HUST), Wuhan, China, in 1992 and 1998, respectively.

He was a Visiting Student from 1996 to 1997 and Research Fellow from 2002 to 2003 all at the University of Liverpool, Liverpool, UK, and a Senior Visiting Researcher at the University of Texas at Arlington, Arlington, USA, in 2010. From 1998 to 2002 he was a Director Engineer with XJ Electric Co. Ltd. in China. In 2003, he joined the HUST and now is a Professor with the School of Electrical and Electronics Engineering, HUST. His current research interests include renewable energy integration, energy storage, multi-terminal HVDC and power system operation and control.

Yuhang Wu obtained the B.E. degree in electrical engineering from Sichuan University, Sichuan, China, in 2021. He is currently pursuing the Ph.D. degree in electrical engineering with Shanghai Jiao Tong University, Shanghai, China. His research interests include energy storage system control in power system.
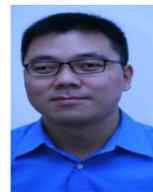
Qiuwei Wu (M,08-SM,15) obtained the PhD degree in Power System Engineering from Nanyang Technological University, Singapore, in 2009.

He has been working at Department of Electrical Engineering, Technical University of Denmark (DTU) since Nov. 2009 (PostDoc Nov. 2009-Oct. 2010, Assistant Professor Nov. 2010-Aug. 2013, Associate Professor since Sept. 2013). His research interests are operation and control of power systems with high penetration of renewables, including wind power modelling and control, active distribution networks, and operation of integrated energy systems. He is an Editor of IEEE Transactions on Smart Grid and IEEE Power Engineering Letters. He is also an Associate Editor of International Journal of Electrical Power and Energy Systems, and Journal of Modern Power Systems and Clean Energy. He is a subject editor for IET Generation, Transmission & Distribution, and IET Renewable Power Generation.